Analysis of Microvasculature in Nonhuman Primate Macula With Acute Elevated Intraocular Pressure Using Optical Coherence Tomography Angiography

Mihyun Choi,[1] Seong-Woo Kim,[1] Thi Que Anh Vu,[2] Young-Jin Kim,[3] Hachul Jung,[3] Donggwan Shin,[4] Heejong Eom,[4] Young Ho Kim,[1] Cheolmin Yun,[1] and Yong Yeon Kim[1]

[1]Department of Ophthalmology, Korea University Medicine, Seoul, Republic of Korea
[2]Department of Ophthalmology, Hanoi Medical University, Hanoi, Vietnam
[3]Medical Device Development Center, Osong Medical Innovation Foundation, Cheongju, Chungbuk, Republic of Korea
[4]Laboratory Animal Center, Osong Medical Innovation Foundation, Cheongju, Chungbuk, Republic of Korea

Correspondence: Seong-Woo Kim, Department of Ophthalmology, Korea University Guro Hospital 148, Gurodong-ro, Guro-gu, Seoul 08373, Republic of Korea;
ksw64723@korea.ac.kr.
Yong Yeon Kim, Department of Ophthalmology, Korea University Guro Hospital 148, Gurodong-ro, Guro-gu, Seoul 08373, Republic of Korea;
yongykim@korea.ac.kr.

Received: September 2, 2021
Accepted: November 24, 2021
Published: December 21, 2021

Citation: Choi M, Kim S-W, Vu TQA, et al. Analysis of microvasculature in nonhuman primate macula with acute elevated intraocular pressure using optical coherence tomography angiography. *Invest Ophthalmol Vis Sci.* 2021;62(15):18.
https://doi.org/10.1167/iovs.62.15.18

Purpose. To investigate responses of macular capillary vessel area density (VAD) of superficial and deep retinal vascular plexuses to elevations in intraocular pressure (IOP) in cynomolgus macaque monkeys using optical coherence tomography angiography (OCTA).

Methods. In five general anesthetized male cynomolgus monkeys, the IOP was increased incrementally by 10 mmHg from baseline (10 mmHg) to 70 mmHg and then decreased back to 10 mmHg (recovery state). Structural OCT (30° × 30°) and OCTA (20° × 15°) centered on the macula were obtained at each IOP and 3, 15, and 30 minutes after recovery. En face images of the superficial vascular complex (SVC) and deep vascular complex (DVC) were extracted, and VAD (%) compared with that at baseline was calculated.

Results. The VADs in the SVC and DVC at baseline and at 30 mmHg IOP were 34.96%, 34.15%, 35.38%, and 30.12%, respectively. The VAD plateaued until 30 mmHg; however, the VAD was affected more in the DVC than in the SVC ($P = 0.008$) at 30 mmHg. It showed a significant reduction at 40 mmHg (16.52% SVC, $P = 0.006$; 18.59% DVC, $P = 0.012$). In the recovery state, the SVC showed full retention of baseline VAD, but the DVC maintained VAD approximately 70% of that at baseline. Structural OCT showed hyperreflectivity in the nuclear layer, retinal swelling, and an undifferentiated ellipsoid zone from 50 mmHg.

Conclusions. Despite physiological autoregulation, perifoveal microcirculation was affected at high IOP ≥ 40 mmHg, especially in the DVC, which explains the pathological mechanism of macular vulnerability in ischemic diseases.

Keywords: microcirculation, angiography, optical coherence tomography, retina, intraocular pressure

The blood supply to the neurosensory retina is crucial for adequate metabolic exchange. The retina is an organ with high metabolic demand, exceeding that of the brain. In the human retina, the superficial vascular complex (SVC) consists of the superficial vascular plexus (SVP) and radial peripapillary capillary (RPC), which originate from the central retinal artery and provide vertical anastomosis to two deeper capillary networks, known as the intermediate capillary plexus (ICP) and the deep capillary plexus (DCP).[1,2] The SVP is comprised of large arteries, arterioles, capillaries, venules, and veins in the ganglion cell layer (GCL) and provides vascular supply to the RPC, parallel to the nerve fiber layer (NFL) and deep vascular plexus including ICP and DCP.[3] During the development of the primate fovea, the SVP develops a perifoveal capillary ring with a foveal avascular area prior to foveal depression and sprouts into deeper vascular plexuses.[2] This foveal avascular zone (FAZ) is often affected in glaucoma and ischemic diseases, such as diabetic retinopathy and retinal vascular obstruction.[4–6]

In response to metabolic demand, autonomic innervation of the choroidal vessels controls vasodilation and vasoconstriction to maintain the blood supply; however, the inner retina lacks such innervation and depends solely on autoregulation mediated by the local vasoactive peptides.[7] During the fluctuation of blood pressure (BP) or intraocular pressure (IOP), autoregulation helps maintain the flow in large vessels and capillaries until overwhelmed.[8] Various laboratory studies using optical coherence tomography angiography (OCTA) have been conducted to investigate the vascular response in terms of increased IOP,[9–11] mainly in small animal models, such as rats.[8,12–14] However, foveal and perifoveal microcirculation, both of which are sensitive to ischemic events, have been relatively less studied.

Nonhuman primates' foveal depression and foveal and perifoveal vascular plexuses are quite similar to those of humans and therefore can be used for structural and vascular investigations.[15,16] In the current study, we aimed to investigate the effects of increased IOP on the perifoveal

capillary and retinal thickness in a cynomolgus macaque monkey.

Methods

This study was approved by the Institutional Animal Care and Use Committee of the Osong Medical Innovation Foundation and adhered to the ARVO Statement for the Use of Animals in Ophthalmic and Vision Research.

Animal Preparation

The subjects of the experiment were five male cynomolgus monkeys (*Macaca fascicularis*) obtained from the Korea National Primate Research Center, Jeongeup-si, Korea. They were bred in a specific pathogen-free area and had a mean age of 55 ± 6.66 months (range, 51–67) and mean weight of 28.47 ± 3.88 kg (range, 23.0–33.2). The monkeys underwent general anesthesia via an intramuscular injection of atropine (0.04 mg/kg), ketamine (7 mg/kg), and medetomidine (60 µg/kg). They were then placed in the supine position and intubated with an orotracheal tube. Anesthesia was maintained with sevoflurane (1.5%–2.5%), and proper hydration was maintained with normal saline (2–3 mL/kg/h). Mean arterial blood pressure (MAP) was monitored non-invasively using an upper arm cuff (Drägerwerk, Lübeck, Germany). The MAP and mean ocular perfusion pressure (MOPP) were calculated based on the following formulas: MAP = diastolic BP + 1/3(systolic – diastolic BP) and MOPP = 2/3(MAP) – IOP.[17] During the experiment, respiratory rate, pulse rate, and blood oxygen saturation were monitored. The monkeys were covered with a warm blanket (39°C), and their body temperature was maintained at 36.8° to 37.5°C. After general anesthesia, the axial length and IOP were measured five times using A-scan ultrasound biometry (SW-1000; Suoer, Foshan Shi, China) and a rebound tonometer (IC200; iCare Finland, Helsinki, Finland) before IOP was controlled. The average ± SD systolic and diastolic BPs were 98 ± 17 mmHg and 55 ± 16 mmHg, respectively, and the average MAP was 88 ± 21 mmHg. The monkeys were placed in the decubitus position prior to undergoing OCTA.

Control of Intraocular Pressure

One eye from each of the five monkeys was included in the experiment. Before IOP control, OCTA was performed in each individual, and a 23-gauge port (DORC, Zuidland, The Netherlands) was inserted at the inferotemporal limbus, as well as an infusion line that continuously supplied balanced salt solution (Alcon; Fort Worth, TX, USA), was connected. The target IOP was achieved using a precalibrated, vented-gas forced infusion (VGFI) system (DORC, Zuidland, The Netherlands) connected to the infusion line.[18] The target IOPs were from 10 mmHg (baseline) to 70 mmHg, which were achieved by increasing the IOP in increments of 10 mmHg and confirmed with a rebound tonometer.

Experimental Protocol

Following port insertion, the IOP was set at 10 mmHg at baseline and increased in increments of 10 mmHg up to 70 mmHg. At each IOP level, the pressure was maintained for 3 minutes, after which OCTA was obtained. At maximal IOP (70 mmHg), the pressure was maintained for 3 minutes in three eyes of three monkeys (group 1) and for 30 minutes in two eyes of two monkeys (group 2). Then, the infusion line was removed from the port, the flow at the port line was checked, and the pressure was lowered to 10 mmHg and connected to the port again, which was defined as the recovery state. In the recovery state, OCTA was obtained three times as follows: 3 minutes (R1), 15 minutes (R2), and 30 minutes (R3) after lowering the IOP.

Structural OCT and OCTA were performed using a spectral-domain OCT device (Spectralis OCT2; Heidelberg Engineering, Heidelberg, Germany). The OCT images were acquired with a volume scan of 7.4 × 7.4-mm (30° × 30°) areas centered on the macula and included 61 B-scans averaging 45 repeated images. The OCTA images were set to scan 4.9 × 3.7-mm (20° × 15°) areas centered on the macula and included 384 vertical B-scans averaging seven repeated images. The scan area at baseline (10 mmHg) was selected as the reference image, and OCT and OCTA images at the same location were obtained throughout the experiment using the auto-rescan function. As the monkeys were placed in the decubitus position, OCT and OCTA images were rotated to the right position before analysis.

OCT and OCTA Image Processing and Analysis

Segmentation of the individual retinal layers in the internal limiting membrane, NFL, GCL, inner plexiform layer (IPL), inner nuclear layer (INL), outer plexiform layer (OPL), outer nuclear layer (ONL), external limiting membrane, and Bruch's membrane on structural OCT and OCTA was conducted using the Heidelberg Engineering built-in software (HEYEX). To obtain en face images of the superficial and deep vascular complexes (DVCs), the SVC en face image was segmented from the internal limiting membrane to the IPL, which included the RPC in the NFL but rarely presented in the perifovea,[19] and mainly the SVP in the GCL and IPL, reflecting the inner retinal blood vessels. The DVC was defined from the outer IPL to the OPL, including the intermediate and deep vascular plexuses in the IPL–INL and INL–OPL interfaces, respectively.[1,8] All segmentation lines in every vertical B-scan on structural OCT and OCTA were manually adjusted by a retinal specialist (MC) under the guidance of a senior advisor (SWK). The en face image was exported after applying the projection artifact-removal function in the software, and the region of interest was cropped into 3 × 3-mm images centered on the fovea (Fig. 1; for images from all five monkeys, see Supplementary Figs. S1 and S2).

To quantify the vessel area density (VAD) of the retinal capillaries, the larger vessel in the SVC was selected as a stack and masked in the SVC images (Figs. 1A–1D). The central 0.6-mm-diameter area centered on the fovea was excluded to mitigate the effect of the FAZ on the vessel density measurements (Figs. 1C, 1F).[20] The VAD as the ratio of white (vessel) to black pixels[21] was calculated using ImageJ[22] (National Institutes of Health, Bethesda, MD, USA) after binarization by two graders, and the mean value was used in the analysis (Figs. 1D, 1G). Thickness values of the total retina, NFL, GCL+IPL (GCIPL), INL, OPL, and ONL from each of the nine Early Treatment of Diabetic Retinopathy Study (ETDRS) subfields centered on the fovea were collected for each layer in each subject and averaged (Figs. 1H–1J).

To assess the foveal pit metrics, the thickness profile in the horizontal OCT scan, including the brightest foveal reflex, was extracted. When a bright reflex was absent, the frame containing the thickest outer segment layer was

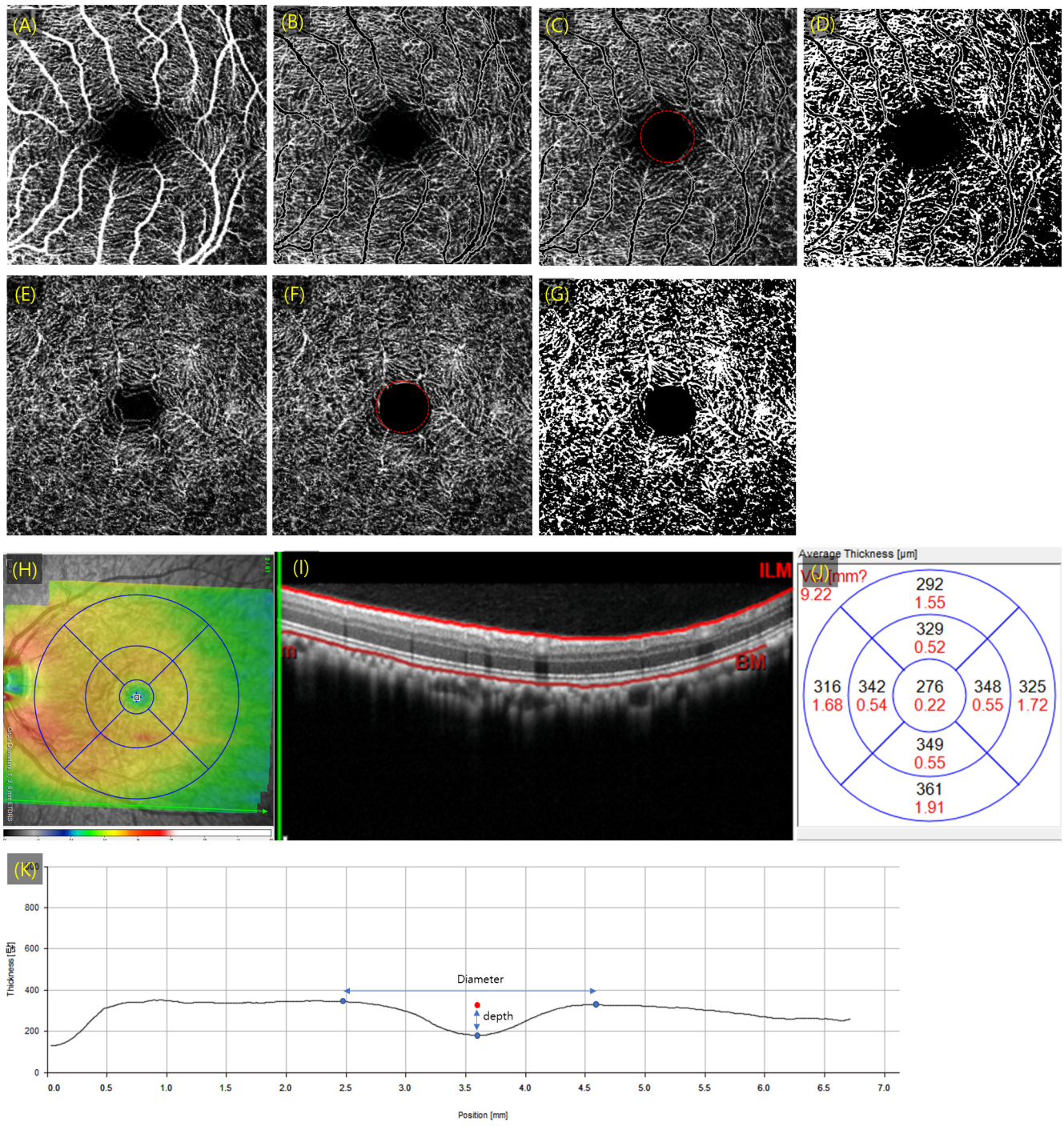

Figure 1. Processing of OCTA en face images (**A–G**) and measurement of retinal thickness (**H–J**). (**A**) Superficial and (**E**) deep vascular complex en face images 3 × 3 mm in size. (**B**) Arterioles and venules selected as a stack and masked in the SVC images. (**C**, **F**) The FAZ (0.6 mm) was excluded in the quantification of VAD. (**D**, **G**) Binarized image. (**H**) Retinal thicknesses measured in nine ETDRS subfields centered on the fovea. (**I**) Layer check and modification in each B-scan. (**J**) Retinal thicknesses in each subfield were obtained and averaged. (**K**) Measurement of the foveal pit metrics. In the thickness profile of foveal pit horizontal OCT, the center and rim of the foveal pit are identified as a location of zero slopes at the center and on both sides of the foveal pit (*blue dot*). Foveal diameter was defined as the rim-to-rim distance, and depth was the difference in thickness between the foveal pit and the mean value of two rims (*red dot*). The maximal slope was the larger angle between the foveal pit and both rims.

chosen.[23,24] In the extracted thickness profile, the center and rim of the foveal pit were identified as the location of zero slopes. Foveal diameter, depth, and maximal slope were recorded (Fig. 1K; for images from all five monkeys, see Supplementary Fig. S3).[25]

Statistical Methods

Data are shown as mean ± standard error of the mean (SEM). Prism 7 (GraphPad Software, San Diego, CA, USA) was used for statistical and graphical analyses. Intraclass correlation

coefficients (ICCs) were evaluated between the two examiners for VAD. Changes in VAD and retinal thickness according to IOPs in each subject were analyzed using a one-way repeated-measures ANOVA (RM-ANOVA) with Greenhouse–Geisser correction, and changes against baseline (IOP at 10 mmHg) were tested using the post hoc Dunnett's test. To compare the responses among multiple retinal thicknesses and VADs, a two-way RM-ANOVA was used to compare changes across IOP levels.

Results

The mean age and body weight were 52.47 ± 6.86 months and 3.82 ± 0.48 kg, respectively. The mean axial length of the eyeball was 18.66 ± 0.56 mm, and the mean IOP after general anesthesia was 8.2 ± 2.8 mmHg. Previously reported normative IOP using a rebound tonometer after ketamine sedation in 14 rhesus macaques was 16 to 18 mmHg. Sevoflurane inhalation during general anesthesia might lower the IOP in this experiment by affecting aqueous flow and extraocular muscle tone, as previously reported.[26,27] ICCs between two graders for VAD were 0.977 in the SVC and 0.933 in the DVC (both $P < 0.001$). Figure 2 presents an example of serial changes in the OCTA images of the SVC and DVC during IOP elevation. Both vascular complexes showed attenuation in smaller vessels at 40 mmHg, and the flow signal in the smaller vessels was greatly reduced at 50 mmHg. At R3, that is, the recovery state 30 min after exposure to maximal IOP (70 mmHg), the SVC recovered to that at the baseline, but partial flow deficit was observed in the DVC. Structural OCT changes were observed from the IOP of 50 mmHg as great flow signal attenuation on OCTA (Fig. 3). At 50 mmHg, hyperreflectivity of the GCIPL, INL, ONL and photoreceptor flattening was observed and more evident at higher IOP. After IOP normalization, the hyperreflectivity of INL, and ONL decreased and ellipsoid zone of the fovea became clear. However, this changes in recovery state were delayed in group 2, which were exposed to maximal IOP for 30 min.

Vessel Area Density

The VADs before port insertion were 36.98% ± 1.55% and 38.74% ± 3.84% in the SVC and DVC, respectively, which were not significantly different from those at 10 mmHg ($P = 0.118$ and $P = 0.09$, respectively). The mean VADs of the retinal capillaries excluding larger vessels are illustrated in Figures 4A and 4B. Analysis of the VAD in the SVC and DVC showed that IOP elevation significantly affected both vascular complexes (one-way RM-ANOVA, both $P < 0.0001$). The VADs in the SVC and DVC were 34.96% ± 0.69% and 34.15% ± 0.69% at baseline and 35.38% ± 0.96% and 30.12% ± 1.75% at 30 mmHg, respectively; they showed no significant changes in post hoc analyses ($P = 0.966$ and $P = 0.114$, respectively). At 40 mmHg, both vascular complexes showed decreases in VAD (SVC: 16.52% ± 2.45%, $P = 0.006$; DVC: 18.59% ± 2.18%, $P = 0.012$), which was significantly lowered at 50 mmHg (5.99% ± 0.69% and 4.57% ± 0.62%, respectively; both $P < 0.001$). The relative vessel densities (Fig. 4C) at 20, 30, 40, 50, and 60 mmHg IOP proportional to those at baseline were 98.55%, 101.9%, 47.24%, 17.32%, and 1.77% in the SVC and 96.88%, 86.46%, 53.06%, 12.95%, and 6.4% in the DVC. There was no difference in relative vessel density between the two vascular complexes according to the IOP (two-way RM-ANOVA, $P = 0.332$), but post hoc multiple comparisons showed differences of 30 mmHg between the two layers ($P = 0.008$). The fitting curves in the scatterplot of relative vessel density by ocular perfusion pressure of the two vascular complexes showed a similar pattern (Fig. 4D).

The relative VADs of the recovery state for each subject are shown in Figures 4E and 4F. In subjects with the 3-minute exposure to maximal IOP and immediate IOP normalization after OCTA images were taken at maximal IOP (group 1, $n = 3$), the relative VADs in the SVC increased in all three subjects at R1 (108.53%, 101.29%, and 102.63%, respectively). In group 2 ($n = 2$), which was exposed to an IOP of 70 mmHg for 30 minutes, both subjects showed decreases in relative VAD in the SVC to 38.5% and 52.3% at R1, but

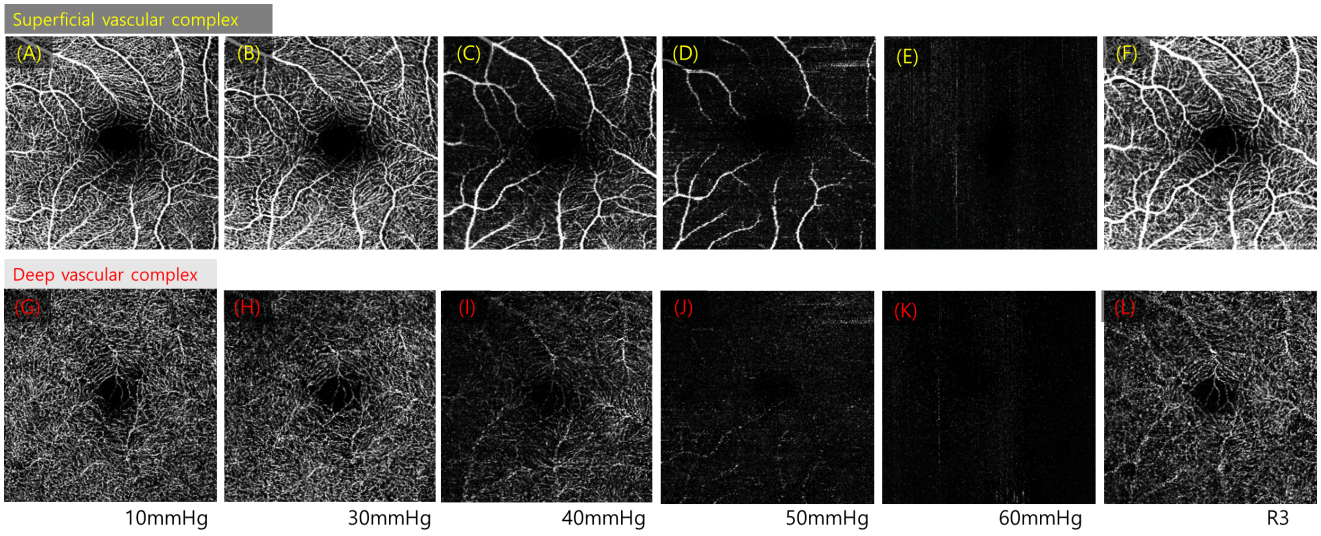

Figure 2. An example of serial changes in OCTA images of the SVC and DVC during IOP elevation. (**A**–**F**) Superficial vascular complex; (**G**–**L**) deep vascular complex. (**A**, **B**) Baseline. At 30 mmHg, a focal flow deficit can be observed in the DVC (**H**) but the vascular shape in the SVC is intact (**B**). From 40 mmHg, a definite capillary flow deficit, particularly at the fine end of capillaries, is observed (**C**, **I**). Only larger vessels (arteriole or venules) show flow signal above 50 mmHg in the SVC (**D**), and almost no flow signal, or a dot artifact only, is observed at 60 mmHg. (**F**, **L**) In the recovery state, all large vessels and the SVC seemed to recover their signal intensity, but a focal flow deficit can be observed in the DVC.

Investigative Ophthalmology & Visual Science

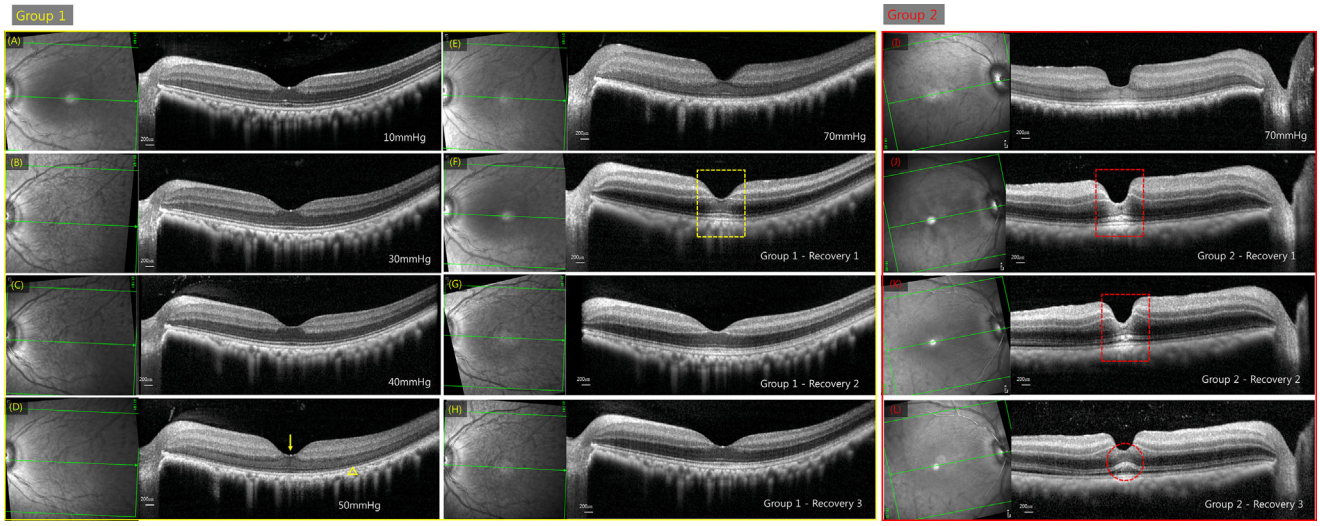

Figure 3. Representative structural OCT changes during IOP elevation and recovery state in group 1 (**A–H**) and group 2 (**I–L**). (**A–C**) No morphological change in the OCT could be detected from baseline to 30 mmHg IOP. The layer-by-layer structure is clearly distinguished, and the inner and outer segments of the photoreceptor are also well observed. (**D**) From 50 mmHg, inner and outer retinal thickening with hyperreflectivity in the GCL, INL, and ONL can be observed. The inner and outer segments of the photoreceptor seem flattened and barely differentiated (*arrowhead*). The relatively low T-shaped signal, which is estimated to be the foveal Müller cell cone structure, can be observed; because of the relatively high signal intensity, the inner ONL seems to be Henle's fiber layer (*arrow*). (**E**) At 70 mmHg, the cell layer haziness further increases, making it difficult to distinguish the layer-by-layer structure. (**F**) After 3 minutes of IOP normalization (R1) in group 1, which was exposed to 70 mmHg for 3 minutes, the haziness of the ONL and INL decreased and hyperreflectivity of the foveal pit persisted (*yellow dot line box*), perhaps indicating relative signal enhancement due to the absence of inner retinal haziness or hyperreflectivity of the ONL in the FAZ. (**G**, **H**) After 15 minutes and 30 minutes of IOP normalization (R2 and R3), gradual decreases in retinal swelling occurred. (**I–L**) After IOP normalization in group 2, which was exposed to 70 mmHg for 30 minutes, inner retinal haziness gradually decreased, but the hyperreflectivity of the ONL in the FAZ (*red dot line box*) persisted, and focal hyporeflective intraretinal fluid can be observed in foveola at 3 and 15 minutes after IOP normalization (R1 and R2). The photoreceptor pulling of the foveal pit displayed reduced retinal swelling (*red dot line circle* in **L**), and subtle subretinal fluid was found at R2 and R3.

these normalized to 106.1% and 110.2% at R2, respectively. However, in the DVC, the relative VADs decreased to 64.1%, 83.2%, and 74.1% in group 1 at R1, and this decrease continued at R3 to 69.0%, 69.6%, and 71.0%, respectively. In group 2, the decrease in VADs was more severe at R1 by 41.4% and 34.9%, respectively, showing less than half of that at baseline; however, at R3, the relative VADs increased to 63.9% and 68.0%, respectively, similar to those in group 1.

Retinal Thickness and Foveal Pit Metrics

Figure 5 illustrates the effect of IOP elevation on the thickness of the various retinal layers and retinal thickness changes in the recovery state. Total retinal thickness (Fig. 5A) was significantly affected by IOP elevation (one-way RM-ANOVA, $P = 0.019$) due to retinal swelling, although post hoc analysis showed a mild increase at 70 mmHg compared with that at baseline ($P = 0.081$). The GCIPL, INL, and ONL showed an increase in thickness according to IOP elevation (one-way RM-ANOVA, $P = 0.002$, $P = 0.001$, and $P = 0.006$, respectively), but the NFL ($P = 0.190$) and OPL ($P = 0.149$) did not show changes following IOP elevation (Figs. 5B, 5C). Multiple-comparison post hoc analysis showed an incremental increase in INL thickness from 50 mmHg (mean difference from baseline [MDB] = 5.57, $P = 0.011$). Although the multiple-comparison post hoc analysis for GCIPL and ONL showed significant differences from baseline at 70 mmHg (MDB = 15.13 and 19.17, $P = 0.037$ and 0.039, respectively), an increase in thickness was observed from 50 mmHg (MDB = 7.52 and $P = 0.054$) in GCIPL and from 60 mmHg in ONL (MDB = 17.6, $P = 0.08$), which was marked by significant hyperreflectivity and swelling on structural OCT. The relative retinal thicknesses in each subject compared with the thicknesses at baseline in the recovery state are presented in Figures 5D to 5I. In group 2 ($n = 2$), the relative retinal thicknesses of the total retina, NFL, GCIPL, INL, and ONL were thicker than those of the maximal IOP (70 mmHg) at R1, suggesting more swelling induced by ischemia in the retinal tissue.

The depth and maximal slope of the foveal pit (Figs. 6A, 6C) were significantly affected by IOP elevation (one-way RM-ANOVA, $P < 0.001$ and $P < 0.049$, respectively), but foveal pit diameter was not affected (Fig. 6B). Post hoc analysis showed a significant increase in depth at 60 mmHg and slope at 70 mmHg compared with those at baseline ($P = 0.002$ and $P = 0.016$). In the recovery state, the increases in foveal pit depth and slope were observed to be more persistent in group 2 (Figs. 6D–6F).

Discussion

In this study, there was no decrease in the VAD showing autoregulation of retinal vessels up to IOP of 30 mmHg. However, the VADs of the SVC and DVC decreased from 40 mmHg and diminished to 17.32% and 12.95% of the baseline VAD at 50 mmHg. Retinal structural changes were clearly observed after 50 mmHg, when the VAD decreased to less than 20% of the baseline value.

Studies of several animal models to measure retinal blood flow following incremental increases in IOP have reported variable results depending on the animal and experimental models. Zhao et al.[8] measured the vessel density changes

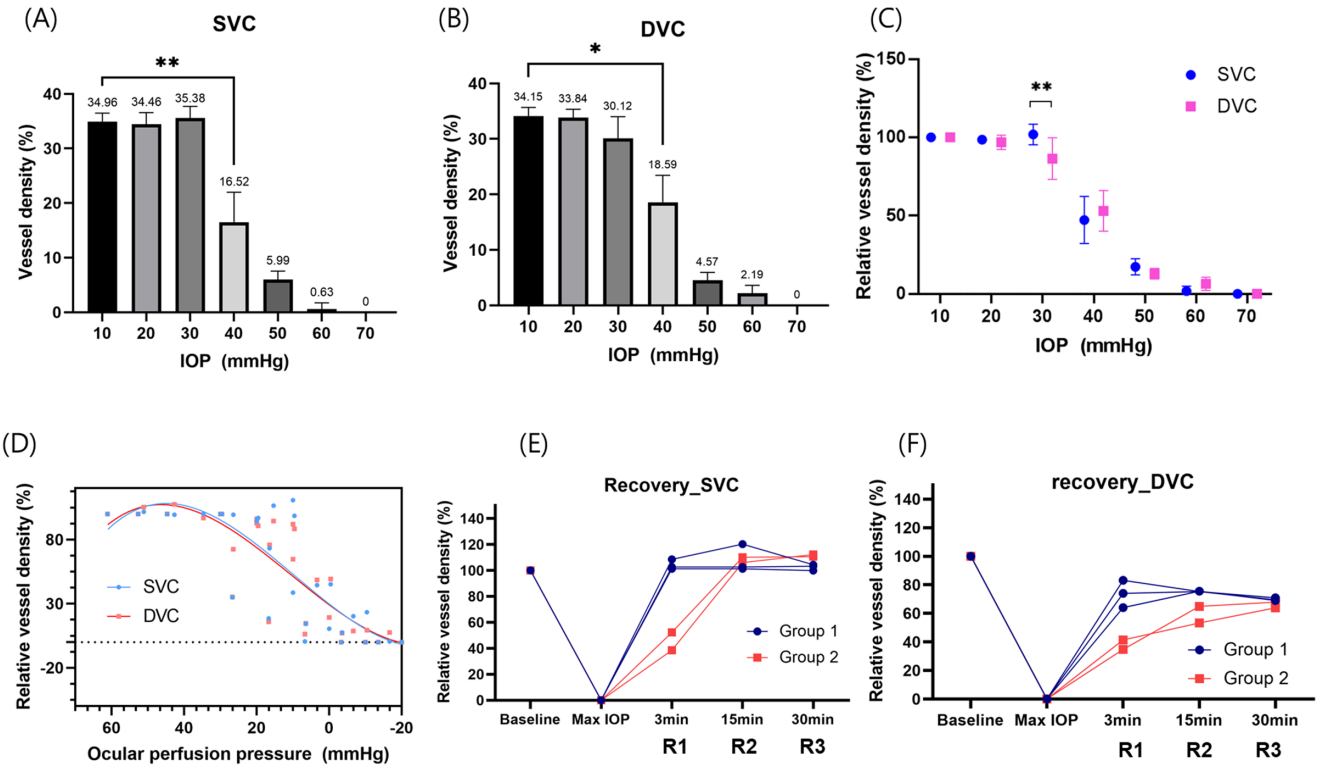

Figure 4. Vessel area density VAD and relative vessel area density (rVAD) following IOP elevation and normalization. (**A**–**C**) Mean values are presented as SEM (*bar*). (**A**, **B**) The VAD of the SVC and DVC from baseline to 70 mmHg. IOP elevation significantly affected both vascular complexes (one-way RM-ANOVA, both $P < 0.0001$). Post hoc analysis found a more significant reduction in VADs from 40 mmHg than those at baseline ($P = 0.006$ in SVC and 0.012 in DVC). At 50 mmHg, the comparison of VADs with those at baseline showed a dramatic reduction (all $P < 0.001$); the P values are not presented in the figure. (**C**) The rVAD of the SVC and DVC at each IOP. The two-way RM-ANOVA and post hoc multiple comparisons showed differences between the two layers ($P = 0.008$) only at 30 mmHg. (**D**) Scatterplot of relative vessel density by ocular perfusion pressure. (**E**) The relative VADs of the recovery state for each subject. Group 1 represents subjects with maximal IOP maintained for 3 minutes with immediate IOP normalization after undergoing OCTA ($n = 3$), and group 2 represents subjects with maximal IOP maintained for 30 minutes ($n = 2$). R1 = 3 minutes after recovery, R2 = 15 minutes after recovery, and R3 = 30 minutes after recovery. *$P < 0.05$ and **$P < 0.01$ in **A**, **B**, and **C**.

in the SVC, ICP, and DCP using OCTA according to the increase in IOP in rat eyes with anterior chamber cannulation and reported that a significant reduction in vessel density was observed above 70 mmHg. For IOPs between 40 and 60 mmHg, the ICP and DCP showed more resistance to IOP than did the SVP. Tan et al.[28,29] used a rat model but raised the IOP using a vascular loop. They reported a reduction in the total retinal blood flow and retinal function measured using electroretinography at IOP ≥ 30 mmHg. In 2021, we reported on the retinal vessel density in a porcine model through an intravitreal port (VGFI system) using OCTA. We observed that the VAD of capillary plexuses decreased to half of the baseline value at 45 mmHg.[30] The 23-gauge port system used in this experiment to control the IOP is a stable and precise method for controlling intravitreal pressure, as cannulation (30-gauge) to the anterior chamber is vulnerable to obstruction due to the small lumen and may cause leakage at the cannulation puncture site.

The fovea is a specialized structure for high-resolution central vision.[31] During development of the primate fovea, the FAZ with the perifoveal capillary ring, made of anastomosing superficial and deep vascular complexes, creates a vascular pattern to match the depression, which maximizes access for photons to reach the photoreceptors, combined with the effect of thinning of the inner retina.[2,32] The vascular structure of the fovea makes the macula vulnerable to ischemic disease and explains the earlier deterioration of vessel density in our results compared with the findings of previous reports.

In our experiment, both capillary plexuses showed a plateau in the VAD up to 30 mmHg, but the relative VAD of the DVC was 86.46%, indicating that it was more affected than that of the SVC (101.9%). Regarding the blood flow pattern in the FAZ, the SVC capillary is directly supplied by the precapillary arteriole, whereas the DVC receives its blood supply from the descending precapillary arteriole from the SVC, and no arterial branches exit vertically from the arterial trunk.[33] The DCP is a laminar, relatively two-dimensional structure composed of capillaries, although the superficial capillary plexus has a denser stack structure with arterioles and venules.[34–36] In previous histological studies of macaque monkeys, the vessels in each of the capillary plexuses converged into tributaries and drained into the main venous trunk, but the DCP in the foveal region usually drains to the main venous trunk, as well.[1,37,38] This consecutive structure suggests a lower outflow pressure in the deeper capillary plexus during IOP elevation and may help explain the susceptibility of DVC to increased IOP.

Previous studies on experimental models of rats and pigs, which do not have the foveal structure, have shown that the retinal blood flow and blood perfusion recovered within

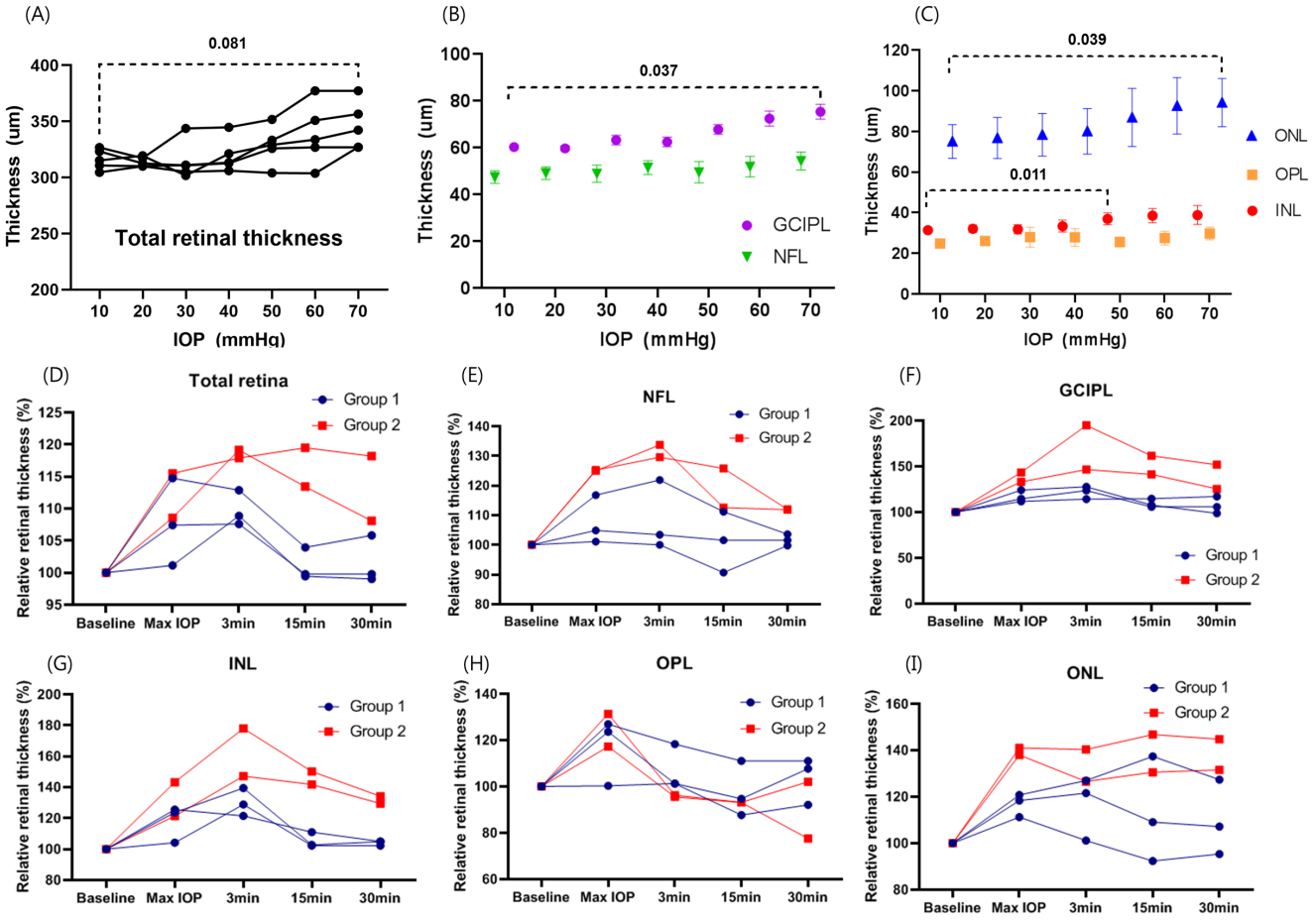

Figure 5. Effect of IOP elevation on the thickness of the various retinal layers and retinal thickness change in the recovery state. (**A**) Total retinal thickness was significantly affected by IOP elevation (one-way RM-ANOVA, $P = 0.019$), although the post hoc analysis of comparisons with baseline values showed a mild increase in thickness at 70 mmHg ($P = 0.081$). From 20 to 60 mmHg, no significant differences were found when compared with baseline values. (**B**, **C**) Thicknesses of GCIPL, NFL, INL, OPL, and ONL following IOP elevation. Mean values are presented as SEM (*bar*). Per the one-way RM-ANOVA, the GCIPL, INL, and ONL showed significant differences according to IOP elevation (one-way RM-ANOVA, $P = 0.002$, $P = 0.001$, and $P = 0.006$, respectively). In post hoc analysis, GCIPL showed a significant increase at 70 mmHg ($P = 0.037$) compared with baseline. INL thickness showed an increase at 50 mmHg ($P = 0.011$), 60 mmHg ($P = 0.015$), and 70 mmHg ($P = 0.057$), and ONL showed significantly greater thickening at 70 mmHg ($P = 0.039$) than at baseline. (**D**–**I**) The relative retinal thickness of the complete retina, NFL, GCIPL, INL, OPL, and ONL for each subject. Group 1 represents subjects with maximal IOP maintained for 3 minutes with immediate IOP normalization after undergoing OCTA ($n = 3$), and group 2 represents subjects with maximal IOP maintained for 30 minutes ($n = 2$). R1 = 3 minutes after recovery, R2 = 15 minutes after recovery, and R3 = 30 minutes after recovery.

30 minutes of normalization of the IOP after induction of ischemic high IOP.[8,12,13,30,39] In the recovery state of our model, even 30 minutes after IOP normalization, the VAD of the DVP recovered to only approximately 70% of the baseline level. It is presumed that mechanical damage or vascular obstruction occurred because of the high IOP, which implies cellular damage by perfusion reduction. Cheung et al.[40] administered an intravitreal injection of 100 µL of saline into two cynomolgus macaque monkeys, and, after ischemic high IOP (98 and >99 mmHg) was achieved, the recovery of vascular flow was observed through OCTA. After IOP normalization (40 minutes later), the SVP flows were 84.2% and 88.9% of the baseline values, and those of the DCP were 68.8% and 78.6% of the baseline values, indicating that flow deflection was more severe and persistent in the DCP. The DCP, which has a laminar structure and receives circulation through the descending arteriole of the SVP, has a higher flow resistance than the SVP,[40] which might affect the recirculation after IOP normalization.

According to the study by Zhao et al.[8] on rats, the retinal thickness decreased at an IOP greater than 80 mmHg in the retinal nerve fiber layer and IPL, but not in the INL and OPL. Although a decrease in thickness due to pressure was expected in this experiment, the GCIPL, INL, and ONL showed an increase in thickness following an increase in IOP, and retinal swelling accompanied by hyperreflectivity was observed on structural OCT, which may be due to ischemic change rather than mechanical pressure. Furthermore, morphological changes in the foveal pit with increasing depth and slope, accompanied by retinal swelling, were observed in this study. Fortune et al.[41] measured peripapillary retinal thickness with a rapid rise in the IOP (to 45 mmHg) in nonhuman primates and reported that the changes were minor. However, in acute retinal ischemia caused by retinal artery occlusion, an increase in hyperreflectivity and indistinguishable layer-by-layer structures in the inner retinal layer resulting in impairment of axoplasmic transport have been reported.[42–46] Additionally, direct

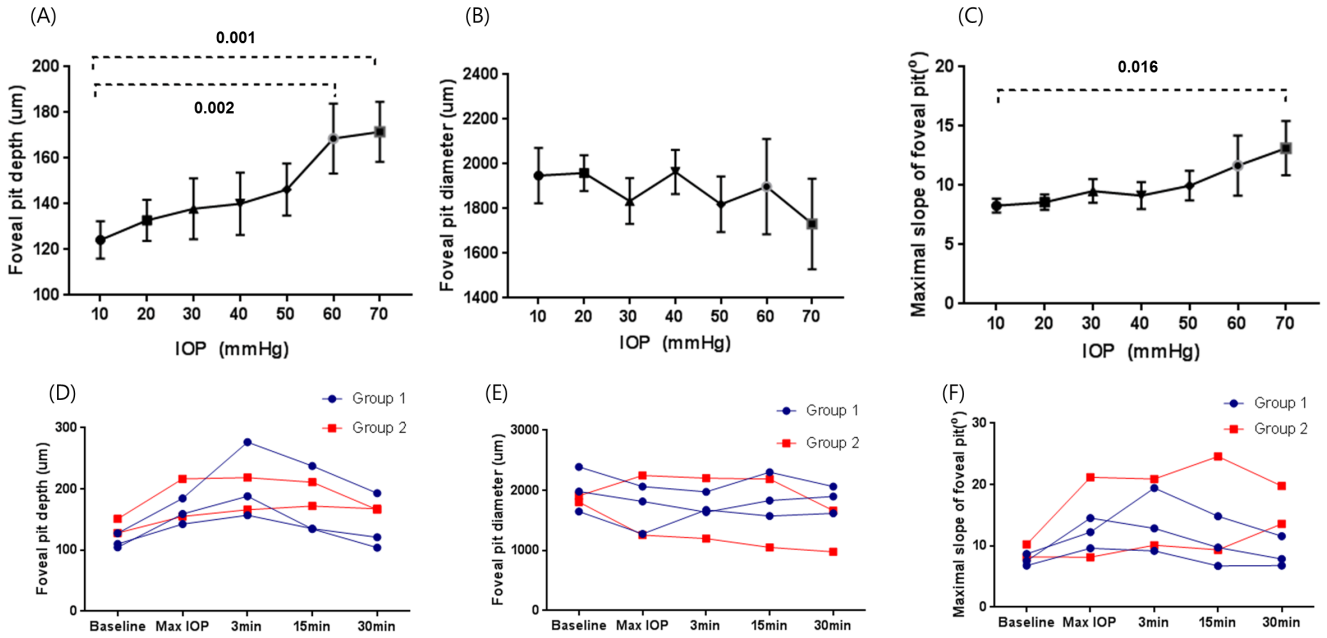

Figure 6. Effect of IOP elevation on the foveal pit morphology. (**A–C**) Mean values are presented as SEM (*bar*). The depth, diameter, and maximal slope of the foveal pit according to IOP (one-way RM-ANOVA, $P < 0.001$, $P < 0.243$, and $P < 0.049$, respectively) showed a significant change in foveal pit curvature at 60 and 70 mmHg. (**D–F**) The depth, diameter, and maximal slope of the foveal pit for each subject at the recovery state. Group 1 represents subjects with maximal IOP maintained for 3 minutes with immediate IOP normalization after undergoing OCTA ($n = 3$), and group 2 represents subjects with maximal IOP maintained for 30 minutes ($n = 2$). R1 = 3 minutes after recovery, R2 = 15 minutes after recovery, and R3 = 30 minutes after recovery.

cytotoxic intracellular swelling may occur because of overexcitation of ionotropic glutamate receptors and neuronal cell depolarization, which causes excess Ca^{2+} and water influx, followed by apoptosis.[47,48]

Interestingly, we observed inner hyperreflectivity in the ONL, which includes the Henle's fiber layer (HFL). HFL are bundles of unmyelinated axons of photoreceptors that run obliquely as a result of lateral displacement in the foveal pit, which makes it a hyporeflective layer in OCT, unlike NFL. Although both HFL and NFL are composed of long cylindrical axons, as a ray of incident light scatters with the same angle as the incident ray, the scattered back light from oblique axons of HFL rarely escapes the pupil and is visualized as hyporeflectivity.[49,50] The impairment of axoplasmic transport and edema in the HFL might change the angle of the axon fiber such that it becomes flatter, and this might affect the light rays that are incident on the HFL and, subsequently, the scattering angle.

Acute retinal edema and subsequent retinal atrophy in central retinal artery occlusion have been reported in animal models and clinically,[45] and the severity of macular edema in the initial phase of ischemia leads to macular atrophy and poor visual acuity.[43,51] In the case of group 2, which was exposed to ischemic high IOP for 30 minutes, the relative retinal thicknesses in the NFL, GCIPL, INL, and ONL versus at baseline were higher than those in group 1 even after IOP normalization. This result made us suspect that neuronal and glial ischemic stress and ischemic cytotoxic damage could be dependent on the exposure time to ischemia and retinal thickness as possible biomarkers of retinal ischemia.

This study has some limitations, including the small number of animals and limited time for evaluating the recovery state after ischemic high IOP. In addition, OCTA images may cause measurement inaccuracies, especially in deeper structures, due to projection artifacts. Unlike methodologies capable of ocular blood flow evaluation, such as laser Doppler velocimetry,[52] OCTA does not provide information on blood flow velocity. In addition, it is possible that the capillary flow at a higher IOP was underestimated because of an increase in retinal structural haziness.

In conclusion, we demonstrated changes in retinal vessel density in the macula of nonhuman primates following IOP elevation to the ischemic state using an OCTA system. We found deterioration in superficial and deep capillary flow at IOP $\geq$ 40 mmHg and a structural change in OCT at an IOP of $\geq$50 mmHg, where the capillary flows of the SVC and DVC were severely reduced to 17.32% and 12.95% of the baseline values, respectively. We believe that our findings can provide substantial information on foveal microvasculature changes due to acute IOP elevation and are meaningful in ophthalmic diseases, including retinal artery obstruction and glaucoma.

Acknowledgments

Supported in part by grants from the Bio & Medical Technology Development Program of the National Research Foundation funded in part by the Korean government, the Ministry of Science, and ICT (NRF-2017M3A9E2056458, 2019M3A9E2030769, and 2020R1A2C1005729).

Disclosure: **M. Choi**; None, **S.-W. Kim**; None, **T.Q.A. Vu**; None, **Y.-J. Kim**; None, **H. Jung**; None, **D. Shin**; None, **H. Eom**; None, **Y.H. Kim**; None, **C. Yun**; None, **Y.Y. Kim**; None

References

1. Campbell JP, Zhang M, Hwang TS, et al. Detailed vascular anatomy of the human retina by projection-resolved optical coherence tomography angiography. *Sci Rep.* 2017;7:42201.
2. Provis JM. Development of the primate retinal vasculature. *Prog Retin Eye Res.* 2001;20:799–821.

3. Henkind P. Radial peripapillary capillaries of the retina. I. Anatomy: human and comparative. *Br J Ophthalmol.* 1967;51:115–123.
4. Ch'ng TW, Gillmann K, Hoskens K, Rao HL, Mermoud A, Mansouri K. Effect of surgical intraocular pressure lowering on retinal structures - nerve fibre layer, foveal avascular zone, peripapillary and macular vessel density: 1 year results. *Eye (Lond).* 2020;34:562–571.
5. Adhi M, Filho MA, Louzada RN, et al. Retinal capillary network and foveal avascular zone in eyes with vein occlusion and fellow eyes analyzed with optical coherence tomography angiography. *Invest Ophthalmol Vis Sci.* 2016;57:OCT486–OCT494.
6. Takase N, Nozaki M, Kato A, Ozeki H, Yoshida M, Ogura Y. Enlargement of foveal avascular zone in diabetic eyes evaluated by en face optical coherence tomography angiography. *Retina.* 2015;35:2377–2383.
7. Riva CE, Sinclair SH, Grunwald JE. Autoregulation of retinal circulation in response to decrease of perfusion pressure. *Invest Ophthalmol Vis Sci.* 1981;21:34–38.
8. Zhao D, He Z, Wang L, et al. Response of the trilaminar retinal vessel network to intraocular pressure elevation in rat eyes. *Invest Ophthalmol Vis Sci.* 2020;61:2.
9. Smith CA, Hooper ML, Chauhan BC. Optical coherence tomography angiography in mice: quantitative analysis after experimental models of retinal damage. *Invest Ophthalmol Vis Sci.* 2019;60:1556–1565.
10. Jiang X, Johnson E, Cepurna W, et al. The effect of age on the response of retinal capillary filling to changes in intraocular pressure measured by optical coherence tomography angiography. *Microvasc Res.* 2018;115:12–19.
11. Zong Y, Xu H, Yu J, et al. Retinal vascular autoregulation during phase IV of the valsalva maneuver: an optical coherence tomography angiography study in healthy Chinese adults. *Front Physiol.* 2017;8:553.
12. Zhi Z, Cepurna WO, Johnson EC, Morrison JC, Wang RK. Impact of intraocular pressure on changes of blood flow in the retina, choroid, and optic nerve head in rats investigated by optical microangiography. *Biomed Opt Express.* 2012;3:2220–2233.
13. Zhi Z, Cepurna W, Johnson E, Jayaram H, Morrison J, Wang RK. Evaluation of the effect of elevated intraocular pressure and reduced ocular perfusion pressure on retinal capillary bed filling and total retinal blood flow in rats by OMAG/OCT. *Microvasc Res.* 2015;101:86–95.
14. Xu J, Li Y, Song S, Cepurna W, Morrison J, Wang RK. Evaluating changes of blood flow in retina, choroid, and outer choroid in rats in response to elevated intraocular pressure by 1300 nm swept-source OCT. *Microvasc Res.* 2019;121:37–45.
15. Wilsey LJ, Reynaud J, Cull G, Burgoyne CF, Fortune B. Macular structure and function in nonhuman primate experimental glaucoma. *Invest Ophthalmol Vis Sci.* 2016;57:1892–1900.
16. Kong X, Wang K, Sun X, Witt RE. Comparative study of the retinal vessel anatomy of rhesus monkeys and humans. *Clin Exp Ophthalmol.* 2010;38:629–634.
17. Van Keer K, Breda JB, Pinto LA, Stalmans I, Vandewalle E. Estimating mean ocular perfusion pressure using mean arterial pressure and intraocular pressure. *Invest Ophthalmol Vis Sci.* 2016;57:2260.
18. Okamoto F, Sugiura Y, Okamoto Y, Hasegawa Y, Hiraoka T, Oshika T. Measurement of ophthalmodynamometric pressure with the vented-gas forced-infusion system during pars plana vitrectomy. *Invest Ophthalmol Vis Sci.* 2010;51:4195–4199.
19. Mase T, Ishibazawa A, Nagaoka T, Yokota H, Yoshida A. Radial peripapillary capillary network visualized using wide-field montage optical coherence tomography angiography. *Invest Ophthalmol Vis Sci.* 2016;57:Oct504–Oct510.
20. Hwang TS, Gao SS, Liu L, et al. Automated quantification of capillary nonperfusion using optical coherence tomography angiography in diabetic retinopathy. *JAMA Ophthalmol.* 2016;134:367–373.
21. Rabiolo A, Gelormini F, Sacconi R, et al. Comparison of methods to quantify macular and peripapillary vessel density in optical coherence tomography angiography. *PLoS One.* 2018;13:e0205773.
22. Schneider CA, Rasband WS, Eliceiri KW. NIH Image to ImageJ: 25 years of image analysis. *Nat Methods.* 2012;9:671–675.
23. Tick S, Rossant F, Ghorbel I, et al. Foveal shape and structure in a normal population. *Invest Ophthalmol Vis Sci.* 2011;52:5105–5110.
24. Mohammad S, Gottlob I, Kumar A, et al. The functional significance of foveal abnormalities in albinism measured using spectral-domain optical coherence tomography. *Ophthalmology.* 2011;118:1645–1652.
25. Dubis AM, Hansen BR, Cooper RF, Beringer J, Dubra A, Carroll J. Relationship between the foveal avascular zone and foveal pit morphology. *Invest Ophthalmol Vis Sci.* 2012;53:1628–1636.
26. Sator-Katzenschlager S, Deusch E, Dolezal S, et al. Sevoflurane and propofol decrease intraocular pressure equally during non-ophthalmic surgery and recovery. *Br J Anaesth.* 2002;89:764–766.
27. Termühlen J, Gottschalk A, Eter N, et al. Does general anesthesia have a clinical impact on intraocular pressure in children?. *Paediatr Anaesth.* 2016;26:936–941.
28. Tan B, MacLellan B, Mason E, Bizheva K. Structural, functional and blood perfusion changes in the rat retina associated with elevated intraocular pressure, measured simultaneously with a combined OCT+ERG system. *PLoS One.* 2018;13:e0193592.
29. Tan B, MacLellan B, Mason E, Bizheva KK. The effect of acutely elevated intraocular pressure on the functional and blood flow responses of the rat retina to flicker stimulation. *Invest Ophthalmol Vis Sci.* 2017;58:5532–5540.
30. Choi M, Kim SW, Ahn S, Vu TQA, Yun C, Kim YY. Relationship between retinal capillary vessel density of OCT angiography and intraocular pressure in pig. *Sci Rep.* 2021;11:8555.
31. Packer O, Hendrickson AE, Curcio CA. Photoreceptor topography of the retina in the adult pigtail macaque (*Macaca nemestrina*). *J Comp Neurol.* 1989;288:165–183.
32. Stone J, Itin A, Alon T, et al. Development of retinal vasculature is mediated by hypoxia-induced vascular endothelial growth factor (VEGF) expression by neuroglia. *J Neurosci.* 1995;15:4738–4747.
33. Snodderly DM, Weinhaus RS. Retinal vasculature of the fovea of the squirrel monkey, *Saimiri sciureus*: three-dimensional architecture, visual screening, and relationships to the neuronal layers. *J Comp Neurol.* 1990;297:145–163.
34. Yu PK, Mammo Z, Balaratnasingam C, Yu DY. Quantitative study of the macular microvasculature in human donor eyes. *Invest Ophthalmol Vis Sci.* 2018;59:108–116.
35. Tan PE, Yu PK, Balaratnasingam C, et al. Quantitative confocal imaging of the retinal microvasculature in the human retina. *Invest Ophthalmol Vis Sci.* 2012;53:5728–5736.
36. Yu PK, Balaratnasingam C, Cringle SJ, McAllister IL, Provis J, Yu DY. Microstructure and network organization of the microvasculature in the human macula. *Invest Ophthalmol Vis Sci.* 2010;51:6735–6743.
37. Snodderly DM, Weinhaus RS, Choi JC. Neural-vascular relationships in central retina of macaque monkeys (*Macaca fascicularis*). *J Neurosci.* 1992;12:1169–1193.
38. Chan G, Balaratnasingam C, Yu PK, et al. Quantitative morphometry of perifoveal capillary networks in the human retina. *Invest Ophthalmol Vis Sci.* 2012;53:5502–5514.

Investigative Ophthalmology & Visual Science

39. Zhi Z, Cepurna W, Johnson E, Shen T, Morrison J, Wang RK. Volumetric and quantitative imaging of retinal blood flow in rats with optical microangiography. *Biomed Opt Express.* 2011;2:579–591.
40. Cheung CMG, Teo KYC, Tun SBB, Busoy JM, Veluchamy AB, Spaide RF. Differential reperfusion patterns in retinal vascular plexuses following increase in intraocular pressure an OCT angiography study. *Sci Rep.* 2020;10:16505.
41. Fortune B, Yang H, Strouthidis NG, et al. The effect of acute intraocular pressure elevation on peripapillary retinal thickness, retinal nerve fiber layer thickness, and retardance. *Invest Ophthalmol Vis Sci.* 2009;50:4719–4726.
42. Matthé E, Eulitz P, Furashova O. Acute retinal ischemia in central versus branch retinal artery occlusion: changes in retinal layers' thickness on spectral-domain optical coherence tomography in different grades of retinal ischemia. *Retina.* 2020;40:1118–1123.
43. Chen SN, Hwang JF, Chen YT. Macular thickness measurements in central retinal artery occlusion by optical coherence tomography. *Retina.* 2011;31:730–737.
44. Ahn SJ, Woo SJ, Park KH, Jung C, Hong JH, Han MK. Retinal and choroidal changes and visual outcome in central retinal artery occlusion: an optical coherence tomography study. *Am J Ophthalmol.* 2015;159:667–676.
45. Ochakovski GA, Wenzel DA, Spitzer MS, et al. Retinal oedema in central retinal artery occlusion develops as a function of time. *Acta Ophthalmol.* 2020;98:e680–e684.
46. Gao Y, Wu D, Liu D, et al. Novel acute retinal artery ischemia and reperfusion model in nonhuman primates. *Stroke.* 2020;51:2568–2572.
47. Spaide RF. Retinal vascular cystoid macular edema: review and new theory. *Retina.* 2016;36:1823–1842.
48. Bringmann A, Uckermann O, Pannicke T, Iandiev I, Reichenbach A, Wiedemann P. Neuronal versus glial cell swelling in the ischaemic retina. *Acta Ophthalmol Scand.* 2005;83:528–538.
49. Lujan BJ, Roorda A, Knighton RW, Carroll J. Revealing Henle's fiber layer using spectral domain optical coherence tomography. *Invest Ophthalmol Vis Sci.* 2011;52:1486–1492.
50. Otani T, Yamaguchi Y, Kishi S. Improved visualization of Henle fiber layer by changing the measurement beam angle on optical coherence tomography. *Retina.* 2011;31:497–501.
51. Kim H, Kim HK, Yang JY, Kim SS. Optical coherence tomography measurement and visual outcome in acute central retinal artery occlusion. *Korean J Ophthalmol.* 2018;32:303–311.
52. Wei X, Balne PK, Meissner KE, Barathi VA, Schmetterer L, Agrawal R. Assessment of flow dynamics in retinal and choroidal microcirculation. *Surv Ophthalmol.* 2018;63:646–664.

Investigative Ophthalmology & Visual Science